To: **Journal of the American Ceramic Society**

Chemical Expansion of Yttrium-Doped Barium Zirconate and Correlation with Proton Concentration and Conductivity

Donglin Han [a, *], Naoyuki Hatada [a], Tetsuya Uda [a, *]

[a] Department of Materials Science and Engineering, Kyoto University,

Yoshida Honmachi, Sakyo-ku, Kyoto 606-8501, Japan

* Corresponding authors: Donglin Han (han.donglin.8n@kyoto-u.ac.jp)

and Tetsuya Uda (uda_lab@aqua.mtl.kyoto-u.ac.jp)

TEL: +81-75-753-5445, FAX: +81-75-753-5284

1

Abstract

Y-doped BaZrO$_3$ (BZY) is a promising candidate as an electrolyte in fuel cells, and attracts increasing attention. In this work, a systematic investigation was performed on microstructure, proton concentration, proton conductivity, and hydration induced chemical expansion in Y-doped BaZrO$_3$. The results revealed that the bimodal microstructure in BaZr$_{0.85}$Y$_{0.15}$O$_{3-\delta}$ was composed of large grains with composition close to the nominal value, and fine grains with large compositional discrepancy. This property is considered to be one of the evidences of phase separation at lower temperature than sintering temperature (1600 $^{\rm o}$C), which hinders the grain growth. Thermal expansion coefficient of BZY was measured for various dopant level, and was determined to be around 10^{-5} K^{-1} in wet and dry argon atmosphere. In addition, chemical expansion effect due to hydration was confirmed by HT-XRD in dry and wet Ar atmospheres, and suggests an interesting relationship between the lattice change ratio and proton concentration, in the BZY system with different Y content. The change ratio of lattice constant due to hydration increased obviously with the proton concentration for the sample containing the Y content of 0.02 and 0.05, but only changed slightly when the Y content was increased to 0.1 and 0.15. However, when the Y content was further increased over 0.2, the change ratio of lattice constant due to hydration starts to increase obviously again. Such results indicate a high possibility that the stable sites of protons in BZY changed with the variation in Y content.

Key words: Fuel cell; Proton conductor; Chemical expansion; Barium zirconate

1. Introduction

Protonic ceramic fuel cells (PCFCs) using proton conductive oxides as electrolytes are promising devices for energy conversion, not only because of their relatively lower operation temperature range (450 – 700 $^{\circ}$C) enabling reduced cost on structural materials, but also an increased efficiency for fuel utilization since water vapor is produced at the cathode in PCFCs.   Several candidates [1, 2] were proposed as the electrolyte in PCFCs, but barium zirconate ($BaZrO_3$) doped with yttrium (Y) is regarded to be the most promising one, benefitted from its high protonic conductivity (> 0.01 Scm^{-1} at 600 $^{\circ}$C) in humid atmosphere [3-6], and excellent chemical stability against CO_2 and H_2O [7, 8].

A lot of works have been dedicated to investigate fundamental properties of Y-doped $BaZrO_3$ (BZY), and also its practical application in PCFCs.   Recently, lattice expansion due to hydration in perovskite oxides, or hydration induced chemical expansion in another word, attracts an increasing attention [9-19], since potential risk of crack in electrolyte, or delamination between the electrolyte and electrodes during the fuel cell operation might thereby be introduced.   A clear chemical expansion behavior in the BZY system was reported by Hiraiwa, *et al*. [12] and Andersson, *et al*. [16] with high temperature X-ray diffraction (HT-XRD) analysis in dry atmosphere on hydrated samples. However, much more precise information on the chemical expansion behavior should be provided through a relevant measurement in a controlled humid atmosphere, but such investigation is lacking.

In addition, although fundamental properties of BZY seem to be well studied, several questions still remained.   A bimodal microstructure was observed by Schober, *et al*. [20] in $BaZr_{0.9}Y_{0.1}O_{3-\delta}$

3

prepared by solid state reaction method. Lately, Imashuku, *et al*. also reported such bimodal microstructure in $BaZr_{0.85}Y_{0.15}O_{3-\delta}$ [21]. However, other information, such as local composition of such bimodal microstructure, has not been reported.

In this work, $BaZrO_3$ doped with various Y content were prepared, and HT-XRD were performed in dry and wet Ar atmospheres to evaluate the hydration induced chemical expansion effect. Then, water content and conductivity were measured to enable a combined discussion on the correlation among these properties. In addition, energy dispersion spectroscopy equipped with a scanning transmission electron microscope (STEM-EDS) was applied to examine local composition of $BaZr_{0.85}Y_{0.15}O_{3-\delta}$ to reveal the character of the bimodal microstructure.

2. Experimental

2.1 Material preparation

$BaZr_{1-x}Y_xO_{3-\delta}$ ($x = 0.02, 0.05, 0.1, 0.15, 0.2, 0.25,$ and 0.3) and undoped $BaZrO_3$ were prepared by a conventional solid state reaction method. Starting materials of $BaCO_3$, ZrO_2, and Y_2O_3 powders were mixed at the desired ratios, and ball-milled for 24 h. Mixtures were pelletized under 9.8 MPa and heat-treated at 1000 ºC for 10 h. The pellets were then pulverized by a mortar, and subjected to ball-milling for 10 h for further pulverizing and mixing. After that, the samples were pelletized under 9.8 MPa again, and kept at 1300 ºC for 10 h for synthesizing. The samples were pulverized by the mortar, and ball-milled for 50 h, and subsequently mixed with a binder (NCB-166, DIC

Corporation, Tokyo, Japan). The mixtures were then pressed into pellets at 392 MPa, and heat-treated at 600 ºC for 8 h to remove the binder. At last, after being buried in sacrificial powders which are mixtures of the relevant synthesized powders (99 wt%) and $BaCO_3$ (1 wt%), the pellet-like samples were heated at 1600 ºC for 24 h in oxygen atmosphere for sintering.

2.2 Characterization

Chemical compositions were determined by inductively coupled plasma atomic emission spectroscopy (ICP-AES) with SPS4000 (Seiko Instruments Inc., Chiba, Japan). Relative density of the sintered pellet-like samples was estimated with Archimedes method. Crystal structure was identified with X-ray diffraction (XRD) analysis using Cu $K\alpha$ radiation with X'Pert-ProMPD (PANalytical, Almelo, Netherland). High temperature XRD (HT-XRD) measurements were performed with the same XRD device using a HTK 1200N high-temperature chamber (Anton Paar, Graz, Austria). Dry or wet ($p_{H_2O} = 0.031\,atm$) argon gas was flowed in the high-temperature chamber. HT-XRD patterns were collected during cooling from 1000 to 30 ºC at an average cooling rate about 1.06 ºCmin^{-1}. Detailed procedures of HT-XRD measurements were described in our previous work. [12] Rietveld refinement was carried out utilizing a commercial software X'Pert HighScore Plus to determine lattice constants. Microstructures were observed by scanning electron microscopy (SEM) and scanning transmission electron microscopy (STEM) with VE-7800 (Keyence Co., Osaka, Japan) and JEM-2100F (JEOL, Tokyo, Japan), respectively. Samples for

STEM observations were thinned by an argon ion (Ar^+) beam using a JEOL EM-09100IS Ion Slicer.

The local composition was identified by STEM with JEOL JED-2300.

Karl-Fischer titration method was applied to determine water content. The pellet-like samples

heat-treated at 1600 ºC for sintering were broken into pieces about 2 mm in length, and hydrated in

wet Ar with a water partial pressure of 0.05 atm for at least 6 days at desired temperature. Readers

are referred to our previous works [22] for detailed procedures.

Conductivity measurements of the pellet-like samples with sputtered platinum (Pt) electrodes were

performed in wet H_2 atmosphere with water partial pressure kept as 0.05 atm. Contributions of bulk

(intra-grain) and grain boundary conduction was determined from the impedance spectra, which were

collected by A. C. impedance spectroscopy in the frequency range from 10 Hz to 7 MHz using a

frequency response analyzer (Solartron SI 1260, Solartron Analytical, Farnborough, UK) with

applied voltage of 100 mV at temperature from 600 to 100 ºC.

3. Results

3.1 Phase identification and microstructure observation

All the samples show single perovskite phases after sintering at 1600 ºC (see **Fig. S1** for XRD

patterns), in agreement with previous reports [23, 24]. The actual chemical compositions

determined by ICP-AES were close to the nominal ones, as given in **Table 1**. In the following text,

the samples of $BaZr_{1-x}Y_xO_{3-\delta}$ will be named as the abbreviations given in the table, *e. g*., BZY20 for

$BaZr_{0.8}Y_{0.2}O_{3-\delta}$.
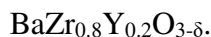
From SEM images of the fractured cross-section shown in **Fig. 1**, it is clear that a bimodal microstructure as a mixture of large and fine grains formed, when the Y content was 0.05, 0.1 and 0.15. Such microstructure was also confirmed from STEM observation on $BaZr_{0.85}Y_{0.15}O_{3-\delta}$ (BZY15), as shown in **Fig. 2**. But, with the Y content increased over 0.2, the grain size turned to be relatively uniform.

Then, STEM-EDS point analysis was applied on BZY15 to determine the local compositions of individual grains. Since the spot size is about 1 nm, the local compositions of the fine grains can also be determined precisely. As shown in **Fig. 3(a)**, the large grains have the composition very close to the nominal value. However, an obvious discrepancy in composition was confirmed for the fine grains (**Fig. 3(b)**) (an example for STEM-EDS analysis is given in supplementary information). It seems that such bimodal structure cannot be treated simply as a mixture of grains just with different size, the difference in compositional homogeneity of the large and fine grains is another important characteristic.

3.2 Proton concentration

The samples hydrated at 300 and 600 ºC in wet Ar ($p_{H_2O} = 0.05$ atm) were subjected to Karl-Fischer titration to determine the proton concentration with the results shown in **Fig. 4**. In general, the proton concentration increased with the increasing Y content. It is because that as

7

given in eqn (1), increasing the Y content resulted in an increasing in oxide ion vacancies ($V_O^{··}$), which benefit the hydration reaction (eqn (2)) to introduce protons ($OH_O^·$).

$$Y_2O_3 + Zr_{Zr}^× + O_O^× \; \rightarrow \; Y_{Zr}' + ZrO_2 + V_O^{··} \tag{1}$$

$$H_2O + V_O^{··} = 2OH_O^· \tag{2}$$
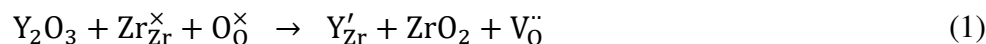
3.3 Thermal and Chemical expansion

Variation of lattice constants, which were determined by Rietveld refinement on the XRD patterns collected through HT-XRD measurements in dry and wet Ar ($p_{H_2O} = 0.031$ atm), against the temperature is shown in **Fig. 5**. Here, only a single cubic perovskite ($Pm\bar{3}m$) model [25] was used to determine the lattice constant. For the samples with a bimodal microstructure, the fitting results should reflect an average effect from the stoichiometric large grains and fine grains with compositional discrepancy. For the samples doped with Y, the lattice constants in wet Ar are larger than those in dry Ar, indicating an expansion effect on lattice volume due to hydration. However, since the dry Ar atmosphere in our apparatus is not absolutely free of water vapour, the Y-doped samples are hydrated slightly during cooling in the low temperature range (30 – 400 ºC), and their lattice constants show a positive deviation from the predicted tendency (broken lines in **Fig. 4**) obtained by extrapolating the data in the high temperature range (700 – 1000 ºC).

Then, thermal expansion coefficients (TECs) of the dehydrated samples in the dry Ar atmosphere were estimated along the broken lines in **Fig. 5**, with the results listed in **Table 1**. TEC for the

undoped $BaZrO_3$ is estimated to be 8.02×10^{-6} K^{-1} in this work, and seems to increase gradually with

the increasing Y content.   But the case in wet Ar is a little complicated, since in addition to the

thermal expansion effect, the chemical expansion induced by the hydration reaction (eqn (2)) also

plays a very important role [16].   But in the relatively low temperature range (*e.g.*, < 300 °C) where

the variation of the amount of water molecules incorporated into BZY with the temperature is

negligibly small [5, 26, 27], the change of the lattice constant in wet Ar is almost parallel with that in

dry Ar.   It means that if excluding the effect from chemical expansion, the value of TEC in wet and

dry Ar is very close.

The lattice constants in dry and wet Ar at 300 and 600 °C are summarized in **Fig. 6** (data at 30 °C are

given in **Fig. S3**), together with the change ratio of lattice constant, which is defined by eqn (3), to

give a quantitative evaluation of the chemical expansion effect [19].   In eqn (3), $a_{wet\ Ar}$ and $a_{dry\ Ar}$

are the lattice constants at 300 or 600 °C obtained in wet and dry Ar atmospheres, respectively.

The extrapolated lattice constants in dry Ar were used here.   It can be seen that the change ratio of

lattice constant due to hydration exhibits a tendency to increase with the increasing Y content,

indicating an enhanced chemical expansion effect.

$$\text{Change ratio of lattice constant} = \frac{a_{wet\ Ar} - a_{dry\ Ar}}{a_{dry\ Ar}} \times 100\% \qquad (3)$$

Deep insight into the behaviour of protons in the crystal lattice of BZY might be provided by

exploring the relationship between the proton concentration and the change ratio of lattice constant.

As shown in **Fig. 7**, when the Y content was very low (0.02 and 0.05), the change ratio of lattice

constant shows an obvious tendency to increase with the increasing proton concentration. However, a plateau appeared when the Y content was between 0.05 and 0.15, that is; although the proton concentrations still increased, the change ratio of lattice constant increased only a little. When the Y content was further increased over 0.2, the change ratio of lattice constant turned to increase significantly again with the increasing proton concentration. This phenomenon is quite interesting. Such special behaviour implies that it is not a simple proportional relation between the degree of chemical expansion effect and the proton concentration. Some other factors also play important roles.

3.4 Bulk and grain boundary conductivities

By analyzing the electrochemical impedance spectra collected in wet H_2, contributions belonging to bulk (intra-grain) and grain boundary conductions are separated [5, 19]. Arrhenius plots of the bulk and grain boundary conductivities of $BaZrO_3$ doped with various Y content are shown in **Fig. 8** and **Fig. 9**, respectively. Here, the bulk and grain boundary conductivities were calculated following eqn. (4). σ is the conductivity. L and S are the thickness and surface area of the pellet-like sample for impedance measurement, respectively. R is the resistance belonging to bulk or grain boundary determined from impedance spectra.

$$\sigma = \frac{L}{R \times S} \tag{4}$$

The contribution from bulk conduction can only be separated at relatively low temperature (an

example of BZY25 is given in the supplementary information).   We here only plotted the bulk and

grain boundary conductivities at 300 $^{\circ}$C in **Fig. 10** for comparison.   The bulk conductivity is very

low for the sample with the Y content of 0.02 and 0.05.   But, when the Y content was increased

from 0.05 to 0.1, the bulk conductivity increased dramatically from 0.61 mScm^{-1} (BZY5) to 2.66

mScm^{-1} (BZY10).   It means that the Y content is just doubled, but the proton conductivity increased

by more than four times.   However, further increasing the Y content over 0.1 does not result in a

large change in the proton conductivity.   Referring to the grain boundary conductivity, it increased

slightly with Y content from 0.02 to 0.15, but a dramatic increase occurred when the Y content was

elevated from 0.15 to 0.2.   Further increase in the Y content results in a decrease in the grain

boundary conductivity.   Apparently, BaZr$_{0.8}$Y$_{0.2}$O$_{3-\delta}$ possess the highest value.

The activation energy (E_a) and pre-exponential factor (A) of the bulk conduction were extracted by

fitting the conductivity data collected between 100 and 200 $^{\circ}$C following eqn. (5).   Here, T is

temperature and k_B is Boltzmann's constant.

$$\sigma T = A \ \exp(\frac{-E_a}{k_B T}) \tag{5}$$

Some literature data with their experimental conditions summarized in **Table 2** were also plotted for

comparison in **Fig. 11**.   Our results agree well with that reported by Bohn, *et al* [28], Imashuku, *et*

al [21], and Yamazaki, *et al* [29], but higher than those reported by Fabbri, *et al*., [23] with a higher

fitting temperature range of 350 – 500 $^{\circ}$C.   As shown in **Fig. 11(a)**, the activation energy of bulk

conduction shows a tendency to increase with the increasing Y content.   And the pre-exponential

11

factor, as shown in **Fig. 11(b)**, increased when the Y content was increased from 0.02 to 0.1, but changed slightly when the Y content was further increased. (The activation energy and pre-exponential factor of the grain boundary conduction are also calculated, and given in supplemental information.)

3.5 Total conductivity

The Arrhenius plots of the total conductivities of $BaZrO_3$ doped with various Y content are shown in **Fig. 12**. For the sake of comparison, **Fig. 13** summarized the value at 400, 500 and 600 °C. It is clear that the total conductivity increased with increasing Y content from 0.02 to 0.2, but decreased when the Y content was higher than 0.2. And $BaZr_{0.8}Y_{0.2}O_{3-\delta}$ has the highest total conductivity at all these three temperatures compared with the other samples containing different Y content. Especially, the value obtained at 500 and 600 °C is larger than 0.01 Scm^{-1}, which is necessary for the application as an electrolyte in fuel cells [30].

In order to check the reproducibility of the total conductivity of $BaZr_{0.8}Y_{0.2}O_{3-\delta}$, five different batches of BZY20 samples were prepared, and their total conductivities are shown in **Fig. 14**. The data marked with the circle symbols are the same as those used in **Fig. 12**. Although a little fluctuation appeared among different preparation batches, in general, reasonably good reproducibility was achieved. And the average value of these five different batches were calculated to be 0.0145 ± 0.0012 Scm^{-1} at 600 °C.

4 Discussion

Compared with BZY20, the grain boundary conductivity of $BaZr_{1-x}Y_xO_{3-\delta}$ ($x = 0.05$, 0.1 and 0.15) is quite low.   Relatively smaller grain size of these samples should be a reason, since the area of grain boundary thereby greatly increased.   That is, it is reasonable to consider that the bimodal microstructure impacts a negative influence on the grain boundary conductivity.   The bimodal microstructure of BZY15 contains the large grains with the composition close to the nominal one, and fine grains possessing significant imhomogeneity in composition.   As far as we know, it is the first time that the precise local composition of such microstructure was determined.   In our previous work [31], we found that when the sintering time at 1600 ^{o}C was increased from 24 h to 100 h, the microstructure of BZY15 turned to be homogeneous.   In addition, by using fine BZY15 powders, which can be prepared with a nitrate freeze drying method [32], even the sintering time at 1600 ^{o}C was shorten to 4 h, a homogeneous microstructure can be achieved.   These results indicate that the equilibrated status of the composition of $BaZr_{0.85}Y_{0.15}O_{3-\delta}$ is a single perovskite phase at 1600 ^{o}C.   Reports on phase observation of $BaZr_{0.9}Y_{0.1}O_{3-\delta}$ (BZY10), which also exhibited a bimodal microstructure in this work, might be informative [33, 34].   Azad, *et al*., [33] observed α-BZY10 phase at relatively low temperature (1500 ^{o}C), which changed to β-BZY10 phase when the sintering temperature elevated to 1720 ^{o}C.   The difference in phase behavior at lower and higher temperature possibly hinders the grain growth, and results in such bimodal microstructure.   But, we do not have direct evidence of the hypothesis, and further investigation in future is needed.

13

Fundamental aspect on the mechanism of proton conduction is always an important and interesting topic. A definite trapping effect of protons in BZY was recently reported by Yamazaki, *et al*. [35] at relatively low temperature (for example, 100 – 200 ºC). Briefly speaking, protons are trapped at the oxide ions near the Y dopant cations, but relatively free at the oxide ions close to the Zr host cations. In the present study, when the Y content is in the range between 0.02 and 0.1, both the activation energy and the pre-exponential factor increased with the increasing Y content. Such behavior of activation energy and pre-exponential factor is reasonable, if we consider the increase of proton concentration and assume a transition status of protons at these temperature ranges, where dominant status of protons is changing from trapped ones to free ones. However, when the Y content is increased over 0.1, although the activation still increases with the increasing Y content, the change in pre-exponential factor is quite small. These results indicate that a simple trapping theory might be available for the system with low Y content (0.02 – 0.1 in this work). For the system containing high Y content, the case seems to be sophisticated rather than a simple trapping effect.

A clear dependence of the chemical expansion behavior on the Y content, which can be divided into three regions, was observed in this study (**Fig. 7**). Since the chemical expansion here is induced by hydration, behavior of protons in the crystal lattice of BZY is expected to be one of the main factors influencing the chemical expansion effect. A recent work by Oikawa, *et al*. revealed a linear relationship between the lattice constant of $BaZr_{0.9}Sc_{0.1}O_{3-\delta}$ and proton concentration [36], implying that if the stable site of protons in the lattice does not change greatly with the proton concentration,

14

an increase in proton concentration should induce a linear behavior of chemical expansion. Thereby, the phenomenon observed in **Fig. 7** suggests possibly different stable sites for protons in BZY with the different Y content. For example, the location of protons might be different between $BaZrO_3$ doped with small Y content (0.02, 0.05) and large Y content (0.15 – 0.3). However, only macroscopic information is available in the present work, establishing detail models might be an interesting topic in the future.

Conclusions

In this work, a systematic investigation on microstructure, proton concentration, proton conductivity, thermal expansion, and hydration induced chemical expansion in Y-doped $BaZrO_3$ was performed. By STEM-EDS analysis, it was found that the bimodal microstructure in $BaZr_{0.85}Y_{0.15}O_{3-\delta}$ is composed of large grains with composition close to the nominal value, and fine grains with large compositional discrepancy. This property is considered to be one of the evidences of phase separation at lower temperature than sintering temperature (1600 ℃), which hinders the grain growth. Behavior of thermal expansion and chemical expansion was investigated by HT-XRD analysis. The thermal expansion coefficient in dry Ar atmosphere was estimated to be 8.02×10^{-6} K^{-1} for undoped $BaZrO_3$, and tended to increase with the increasing Y content. For example, about 1.01×10^{-5} K^{-1} for $BaZr_{0.8}Y_{0.2}O_{3-\delta}$. In addition, an interesting relationship was observed between the proton concentration and the lattice change ratio due to the hydration induced chemical expansion, in

15

the BZY system with different Y content. Such results implied a high possibility that the stable sites of protons in BZY was different between the samples with small Y content (0.02 and 0.05) and those with large Y content (0.15 – 0.3).

Acknowledgement

References

[1] T. Norby, "Solid-State Protonic Conductors: Principles, Properties, Progress and Prospects," *Solid State Ionics*, **125** [1-4] 1-11 (1999).

[2] K.D. Kreuer, "Proton-Conducting Oxides," *Annu. Rev. Mater. Res.*, **33** [1] 333-59 (2003).

[3] Y. Yamazaki, R. Hernandez-Sanchez, and S.M. Haile, "High Total Proton Conductivity in Large-Grained Yttrium-Doped Barium Zirconate," *Chem. Mater.*, **21** [13] 2755-62 (2009).

[4] D. Pergolesi, E. Fabbri, A. D'Epifanio, E.D. Bartolomeo, A. Tebano, S. Sanna, S. Licoccia, G. Balestrino, and E. Traversa, "High Proton Conduction in Grain-Boundary-Free Yttrium-Doped Barium Zirconate Films Grown by Pulsed Laser Deposition," *Nat. Mater.*, **9** [10] 846-52 (2010).

[5] D. Han, Y. Nose, K. Shinoda, and T. Uda, "Site Selectivity of Dopants in $BaZr_{1-y}M_yO_{3-\delta}$ (M = Sc, Y, Sm, Eu, Dy) and Measurement of Their Water Contents and Conductivities," *Solid State Ionics*, **213** 2-7 (2013).

[6] D. Han, N. Hatada, and T. Uda, "Microstructure, Proton Concentration and Proton Conductivity of Barium Zirconate Doped with Ho, Er, Tm and Yb," *J. Electrochem. Soc.*, **163**[6] F470-6 (2016).

[7] K. Katahira, Y. Kohchi, T. Shimura, and H. Iwahara, "Protonic Conduction in Zr-substituted $BaCeO_3$," *Solid State Ionics*, **138** [1-2] 91-8 (2000).

[8] Y. Guo, Y. Lin, H. Shi, R. Ran, and Z. Shao, "A High Electrochemical Performance Proton Conductor Electrolyte with CO_2 Tolerance," *Chin. J. Catal.*, **30** [6] 479-81 (2009).

[9] S. Yamaguchi, and N. Yamada, "Thermal Lattice Expansion Behavior of Yb-doped $BaCeO_3$," *Solid*

State Ionics, **162-163** 23-9 (2003).

[10] J. Wu, R.A. Davies, M.S. Islam, and S.M. Haile, "Atomistic Study of Doped $BaCeO_3$: Dopant Site-Selectivity and Cation Nonstoichiometry," *Chem. Mater.*, **17** [4] 846-51 (2005).

[11] F. G. Kinyanjui, S. T. Norberg, I. Ahmed, S. G. Eriksson, and S. Hull, "In-situ Conductivity and Hydration Studied of Proton Conductors Using Neutron Powder Diffraction," *Solid State Ionic*, **225** 312-6 (2012).

[12] C. Hiraiwa, D. Han, A. Kuramitsu, A. Kuwabara, H. Takeuchi, M. Majima, and T. Uda, "Chemical Expansion and Change in Lattice Constant of Y-Doped $BaZrO_3$ by Hydration / Dehydration Reaction and Final Heat-Treating Temperature," *J. Am. Ceram. Soc.*, **96** [3] 879-84 (2013).

[13] D. Han, M. Majima, and T. Uda, "Structure Analysis of $BaCe_{0.8}Y_{0.2}O_{3-\delta}$ in Dry and Wet Atmospheres by High-Temperature X-ray Diffraction Measurement," *J. Solid State Chem.*, **205** 122-128 (2013).

[14] D. Han, K. Shinoda, and T. Uda, "Dopant Site Occupancy and Chemical Expansion in Rare Earth-Doped Barium Zirconate," *J. Am. Ceram. Soc.*, **97** [2] 643-50 (2014).

[15] D. Han, K. Kojima, M. Majima, and T. Uda, "Synthesis and Conductivity Measurement of Lanthanum Zirconate Doped with Rare Earth Dopants," *J. Electrochem. Soc.*, **161** [10] F977-82 (2014).

[16] A.K.E. Andersson, S.M. Selbach, C.S. Knee, and T. Grande, "Chemical Expansion Due to

Hydration of Proton-Conducting Perovskite Oxide Ceramics," *J. Am. Ceram. Soc.*, **97** [8] 2654-61 (2014).

[17] E. Jedvik, A. Lindman, M. Benediktsson, and G. Wahnström, "Size and Shape of Oxygen Vacancies and Protons in Acceptor-Doped Barium Zirconate," *Solid State Ionics*, **275** 2-8 (2015).

[18] A.K.E. Andersson, S.M. Selbach, T. Grande, and C.S. Knee, "Thermal Evolution of the Crystal Structure of Proton Conducting $BaCe_{0.8}Y_{0.2}O_{3-\delta}$ from High-Resolution Neutron Diffraction in Dry and Humid Atmosphere," *Dalton Trans.*, **44** 10834-46 (2015).

[19] D. Han, K. Shinoda, S. Sato, M. Majima, and T. Uda, "Correlation between Electroconductive and Structural Properties of Proton Conductive Acceptor-Doped Barium Zirconate," *J. Mater. Chem. A.*, **3** [3] 1243-50 (2015).

[20] T. Schober, and H.G. Bohn, "Water Vapor Solubility and Electrochemical Characterization of the High Temperature Proton Conductor $BaZr_{0.9}Y_{0.1}O_{2.95}$," *Solid State Ionics*, **127** [3-4] 351-60 (2000).

[21] Imashuku, T. Uda, Y. Nose, G. Taniguchi, Y. Ito, and Y. Awakura, "Dependence of Dopant Cations on Microstructure and Proton Conductivity of Barium Zirconate," *J. Electrochem. Soc.*, **156** [1] B1-8 (2009).

[22] D. Han, Y. Okumura, Y. Nose, and T. Uda, "Synthesis of $La_{1-x}Sr_xSc_{1-y}Fe_yO_{3-\delta}$ (LSSF) and Measurement of Water Content in LSSF, LSCF and LSC Hydrated in Wet Artificial Air at 300 ºC," *Solid State Ionics*, **181** [35] 1601-6 (2010).

[23] E. Fabbri, D. Pergolesi, S. Licoccia, and E. Traversa, "Does the Increase in Y-Dopant Concentration Improve the Proton Conductivity of $BaZr_{1-x}Y_xO_{3-\delta}$ Fuel Cell Electrolytes?," *Solid State Ionics*, **181** [21-22] 1043-51 (2010).

[24] Y. Ding, Y. Li, W. Deng, W. Huang, and C. Wang, "Variation of Optimum Yttrium Doping Concentrations of Perovskite Type Proton Conductors $BaZr_{1-x}Y_xO_{3-\delta}$ ($0 \leq x \leq 0.3$) with Temperature," *J. Rare Earths*, **31** [10] 1017-22 (2013).

[25] D. Han, K. Kishida, K. Shinoda, H. Inui, and T. Uda, "A Comprehensive Understanding of Structure and Site Occupancy of Y in Y-Doped $BaZrO_3$," *J. Mater. Chem. A*, **1** [9] 3027-33 (2013).

[26] K.D. Kreuer, St. Adams, W. Münch, A. Fuchs, U. Klock, and J. Maier, "Proton Conducting Alkaline Earth Zirconates and Titanates for High Drain Electrochemical Applications," *Solid State Ionics*, **145** [1-4] 295-306 (2001).

[27] Y. Yamazaki, P. Babilo, and S.M. Haile, "Defect Chemistry of Yttrium-Doped Barium Zirconate: A Thermodynamic Analysis of Water Uptake," *Chem. Mater.*, **20** [20] 6352-7 (2008).

[28] H.G. Bohn, and T. Schober, "Electrical Conductivity of the High-Temperature Proton Conductor $BaZr_{0.9}Y_{0.1}O_{2.95}$," *J. Am. Ceram. Soc.*, **83** [4] 768-72 (2000).

[29] Y. Yamazaki, R. Hernandez-Sanchez, and S.M. Haile, "Cation Non-stoichiometry in Yttrium-Doped Barium Zirconate: Phase Behavior, Microstructure, and Proton Conductivity," *J. Mater. Chem.*, **20** [37] 8158-66 (2010).

[30] B.C.H. Steele, and A. Heinzel, "Materials for Fuel-Cell Technologies," *Nature*, **414** 345-52 (2001).

[31] S. Imashuku, T. Uda, and Y. Awakura, "Sintering Properties of Trivalent Cation-Doped Barium Zirconate at 1600 ºC," *Electrochem. Solid-State Lett.* **10**[10] B175-9 (2007).

[32] S. Imashuku, T. Uda, Y. Nose, and Y. Awakura, "Fabrication and Electrical Characterization of 15% Yttrium-Doped Barium Zirconate-Nitrate Freeze Drying Method Combined with Vacuum Heating," *J. Alloys Compd.*, **509** [9] 3872-9 (2011).

[33] A.K. Azad, C. Savaniu, S. Tao, S. Duval, P. Holtappels, R.M. Ibberson, and J.T.S. Irvine, "Structural Origins of the Differing Grain Conductivity Values in $BaZr_{0.9}Y_{0.1}O_{2.95}$ and Indication of Novel Approach to Counter Defect Association," *J. Mater. Chem.*, **18**[29] 3414-8 (2008).

[34] S.B.C. Duval, P. Holtappels, U.F. Vogt, U. Stimming, and T. Graule, "Characterization of $BaZr_{0.9}Y_{0.1}O_{3-\delta}$ Prepared by Three Different Synthesis Methods: Study of the Sinterability and the Conductivity," *Fuel Cells*, **9**[5] 613-21 (2009).

[35] Y. Yamazaki, F. Blanc, Y. Okuyama, L. Buannic, J.C. Lucio-Vega, C.P. Grey, and S.M. Haile, "Proton Trapping in Yttrium-Doped Barium Zirconate," *Nature Mater.*, **12** 647-51 (2013).

[36] I. Oikawa, and H. Takamura, "Correlation among Oxygen Vacancies, Protonic Defects, and the Acceptor Dopant in Sc-Doped $BaZrO_3$ Studied by [45]Sc Nuclear Magnetic Resonance," *Chem. Mater.*, **27** [19] 6660-7 (2015).
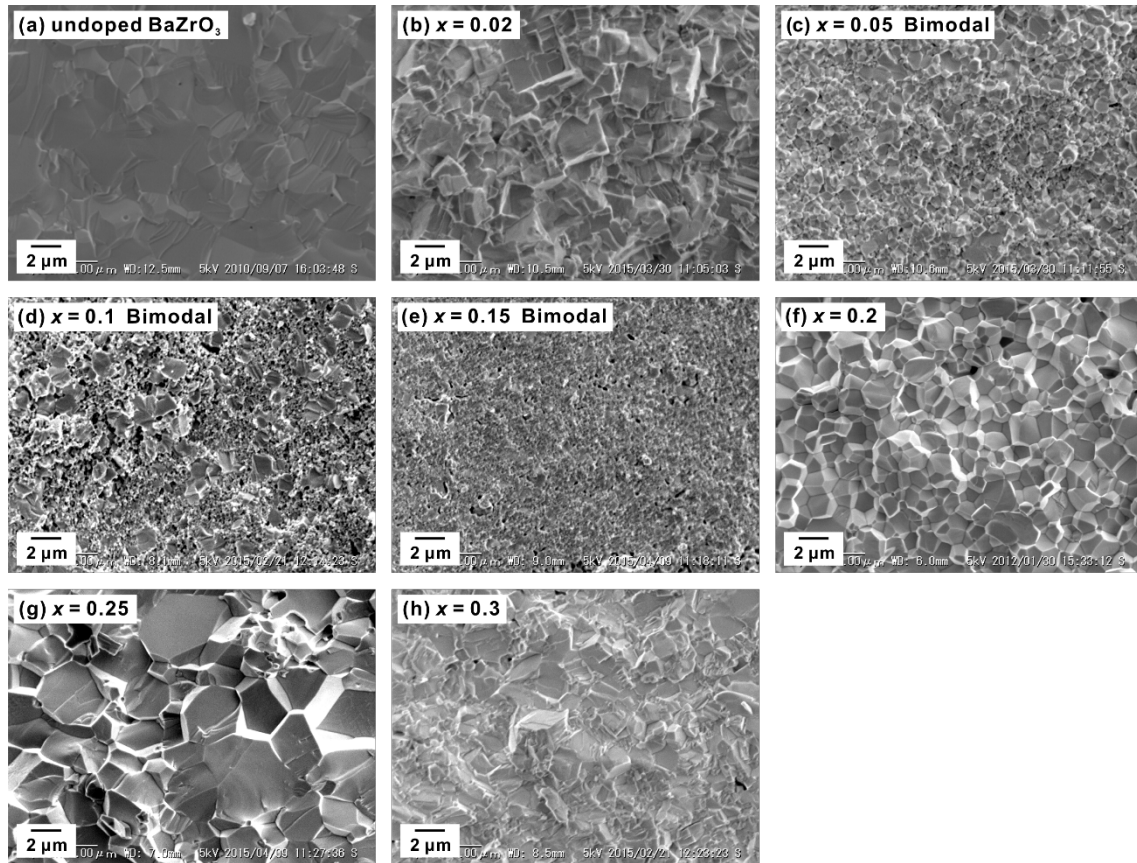
Fig. 1 SEM images of the fractured cross-section of undoped $BaZrO_3$ and $BaZr_{1-x}Y_xO_{3-\delta}$ ($x = 0.02$, 0.05, 0.1, 0.15, 0.2, 0.25 and 0.3).   All the samples were heat-treated at 1600 ℃ in O_2 for 24 h for sintering.
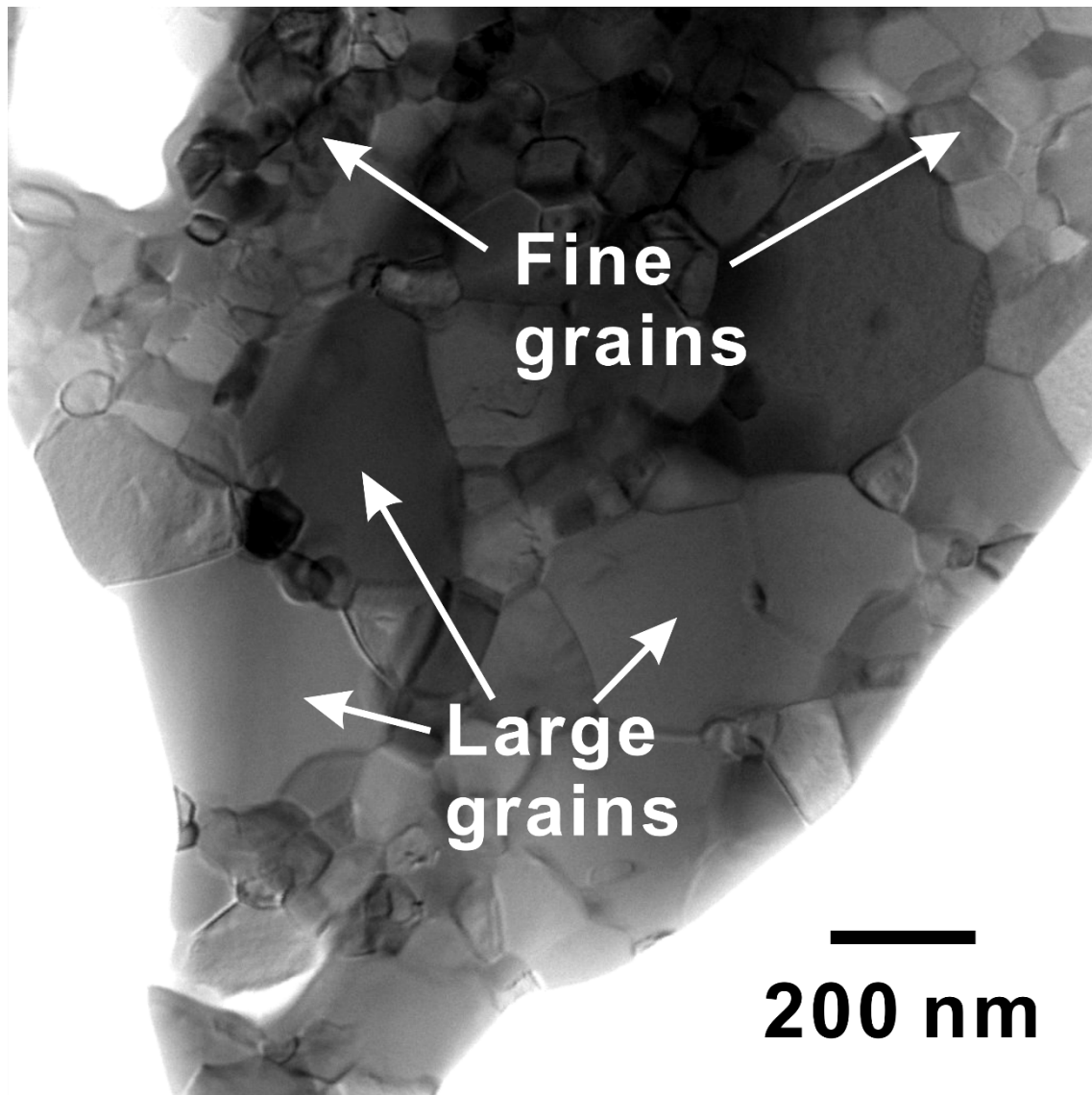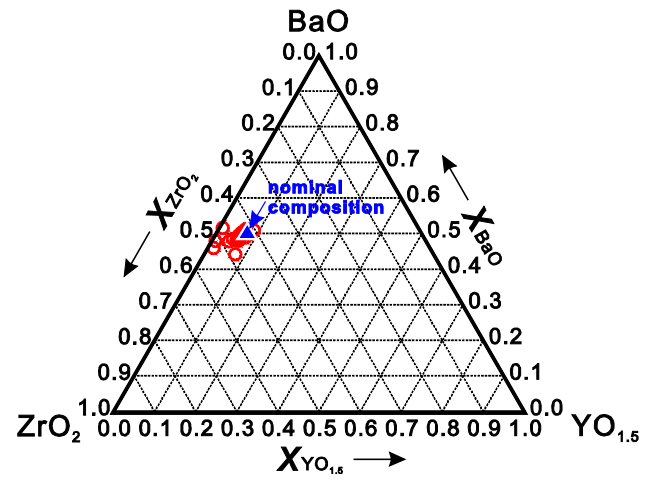
Fig. 2 A bright field STEM (BF-STEM) image of $BaZr_{0.85}Y_{0.15}O_{3-\delta}$ (BZY15), in which a clear co-existence of large grains and fine grains can be seen.
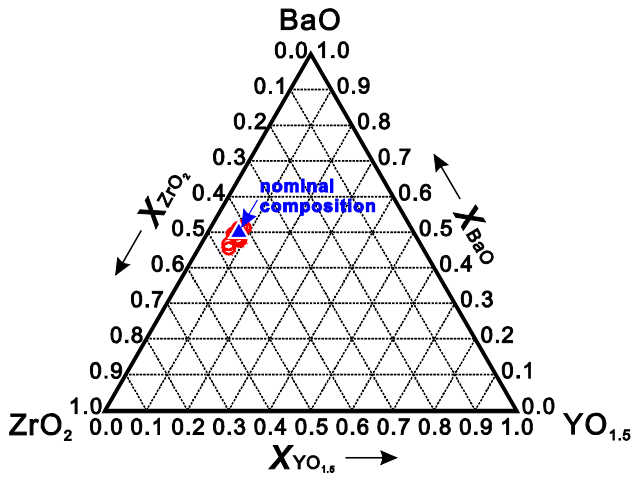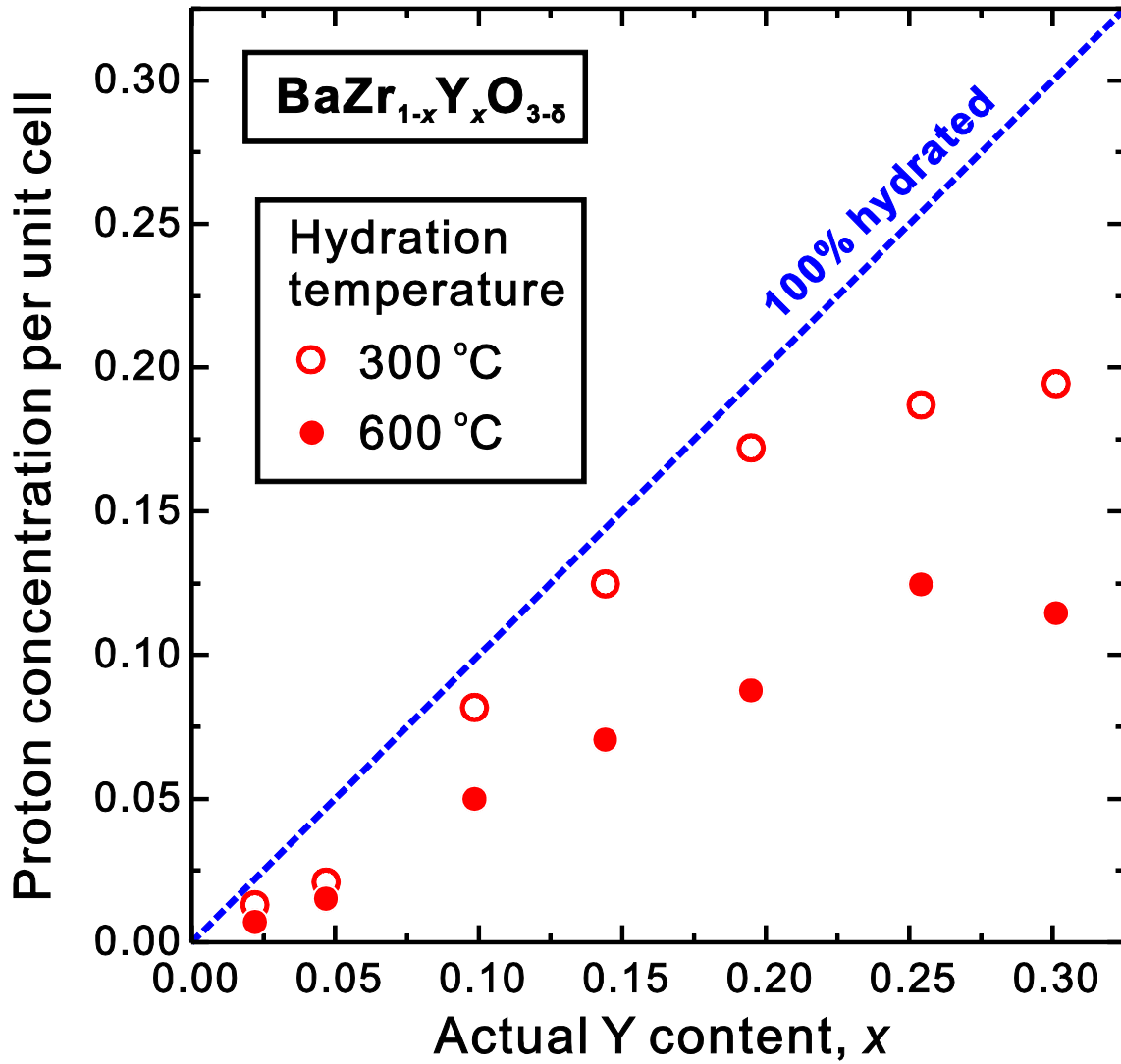
Fig. 3 Results of STEM-EDS point analysis of (a) large grains and (b) fine grains in BaZr$_{0.85}$Y$_{0.15}$O$_{3-\delta}$ (BZY15).

Fig. 4 Proton concentration of $BaZrO_3$ doped with various Y content plotted against the actual Y

content measured by ICP-AES. All the samples were sintered at 1600 ℃ in O_2 for 24 h, and

hydrated at 300 or 600 ℃ in wet Ar ($p_{H_2O} = 0.05$ atm). The proton concentration was calculated

from the water content measured by Karl-Fischer titration method. The data of $BaZr_{0.8}Y_{0.2}O_{3-\delta}$ are

cited from our previous report [5].
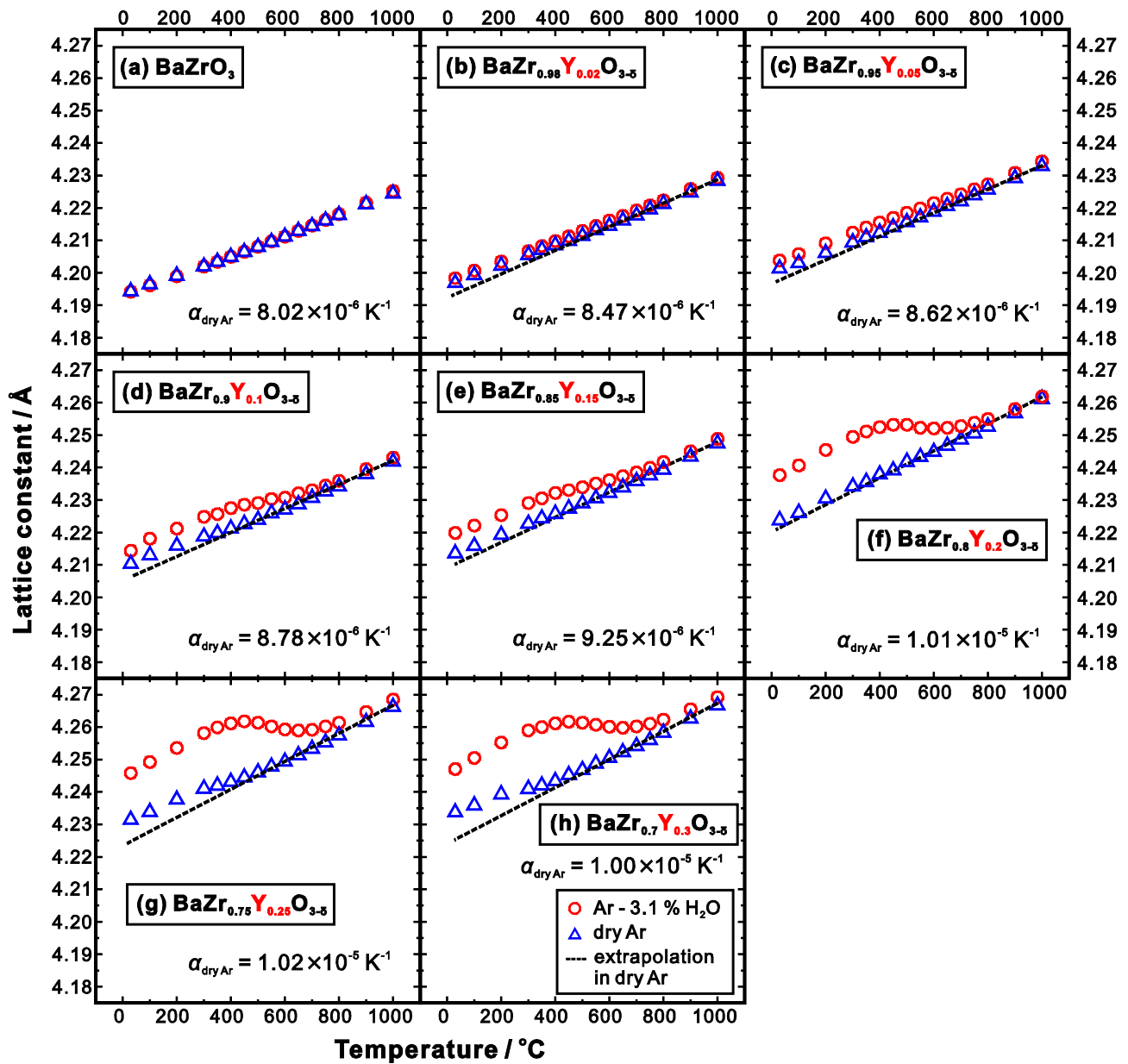
Fig. 5 Variation in lattice constants of undoped $BaZrO_3$ and those doped with various Y content in dry Ar and wet Ar (p_{H_2O} = 0.031 atm) with temperature. All the samples were finally heat-treated at 1600 $°C$ in O_2 for 24 h for sintering.
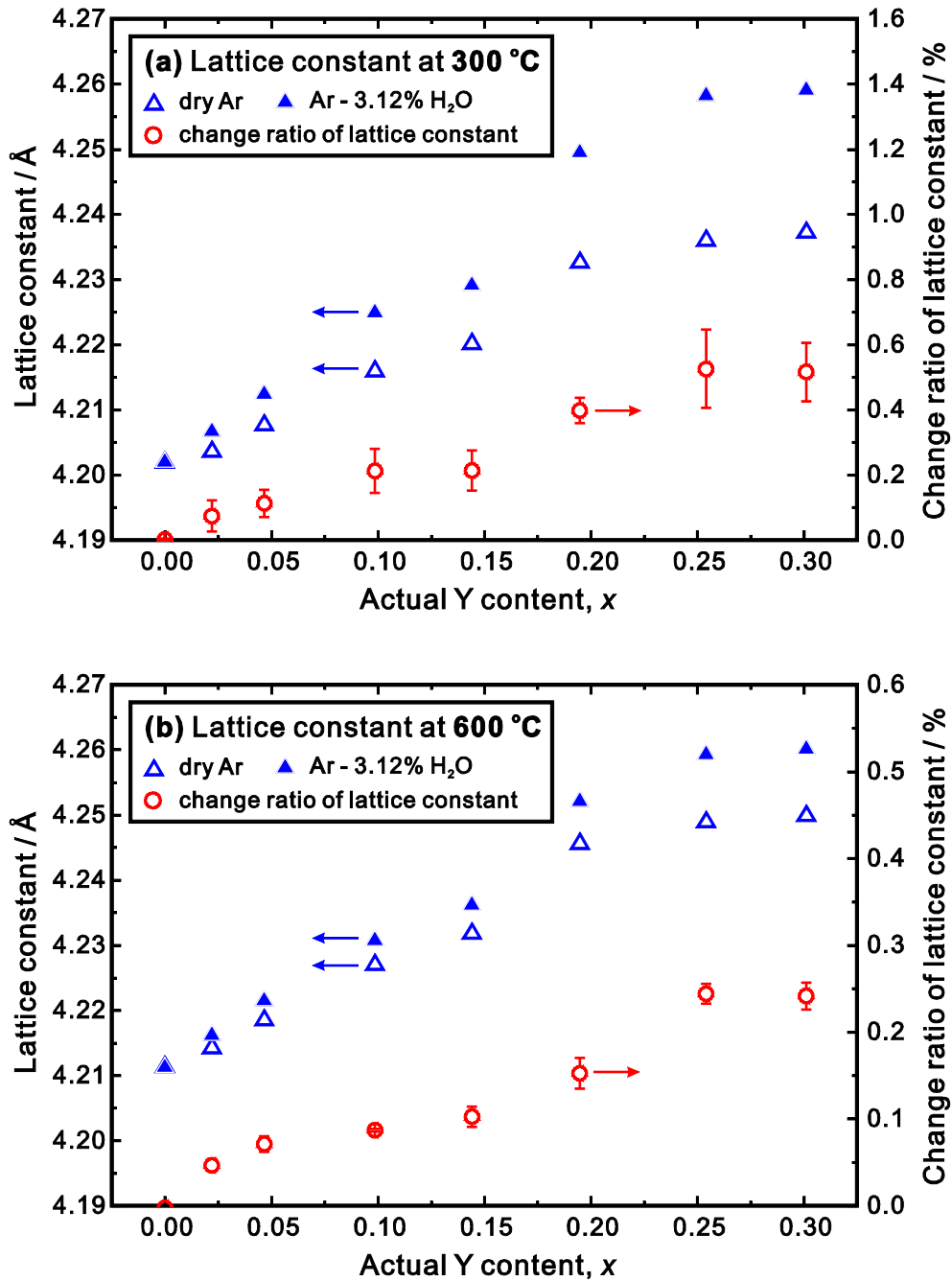
Fig. 6 Lattice constant of BaZrO₃ doped with various Y content determined by HT-XRD

measurements in dry Ar and wet Ar (p_{H_2O} = 0.031 atm) at (a) 300 ℃, and (b) 600 ℃ against the

actual Y content determined by ICP-AES. The lattice constants in dry Ar were determined by

extrapolating the data at high temperature range (700 – 1000 ℃).
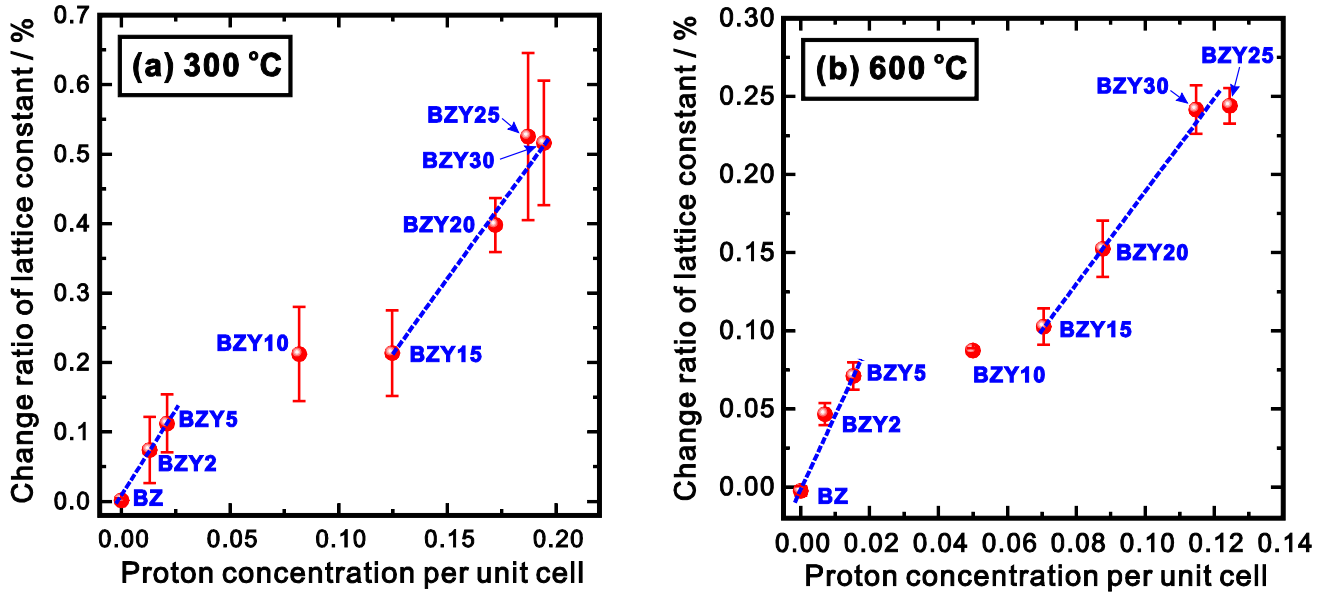
Fig. 7 Relationship between change ratio of lattice constant due to hydration and proton concentration per unit cell at (a) 300 $^{\circ}$C, and (b) 600 $^{\circ}$C. The proton concentration was measured by Karl-Fischer titration method on samples hydrated in wet Ar – 5% H_2O. The change ratio of lattice constant was calculated using the lattice constant determined by HT-XRD in dry Ar (extrapolated) and Ar – 3.1% H_2O. All the samples used here were sintered at 1600 $^{\circ}$C in O_2 for 24 h.
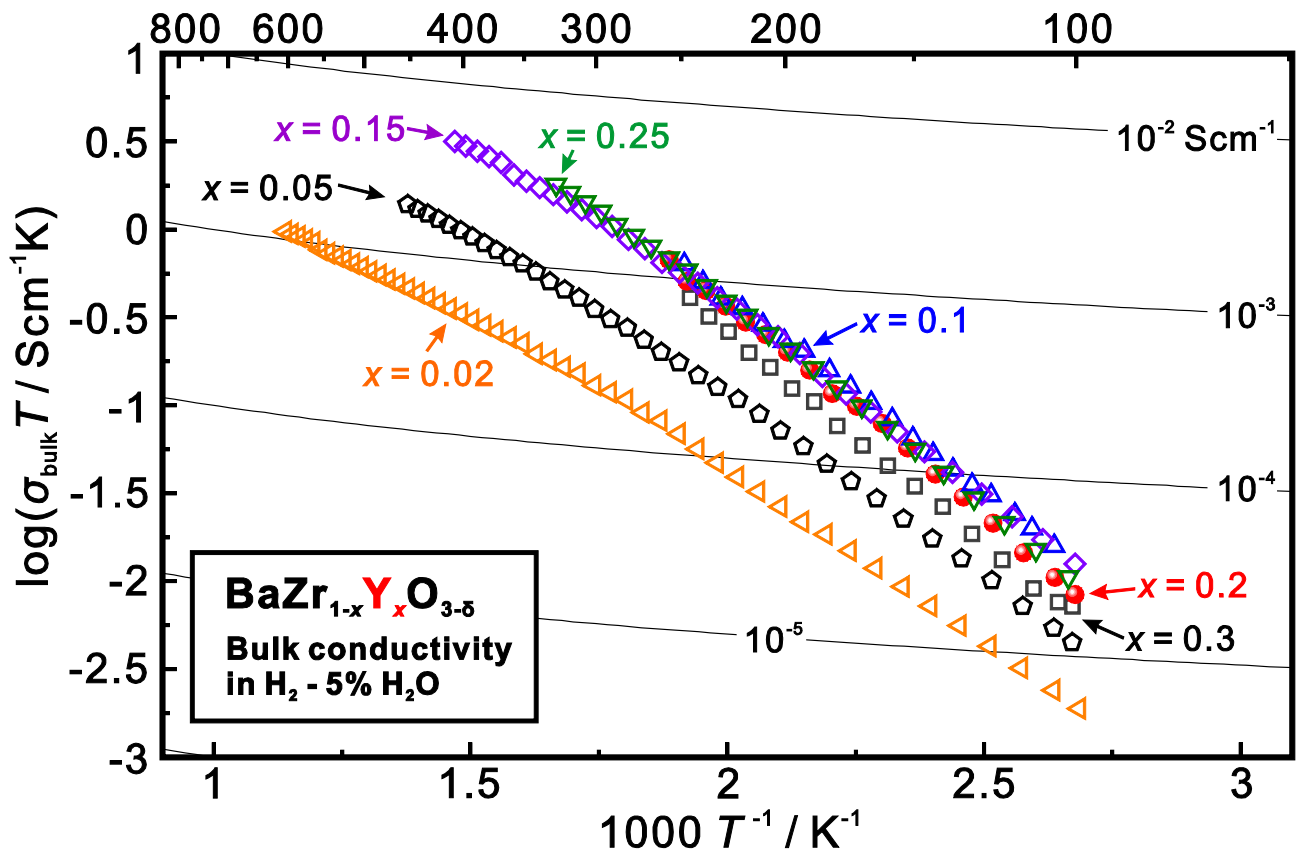
Fig. 8 Arrhenius plots of bulk conductivities of $BaZr_{1-x}Y_xO_{3-\delta}$ (x = 0.02, 0.05, 0.1, 0.15, 0.2, 0.25 and 0.3) in wet H_2 atmosphere with the water vapor pressure of 0.05 atm. All the samples were finally heat-treated at 1600 ℃ in O_2 for 24 h for sintering.
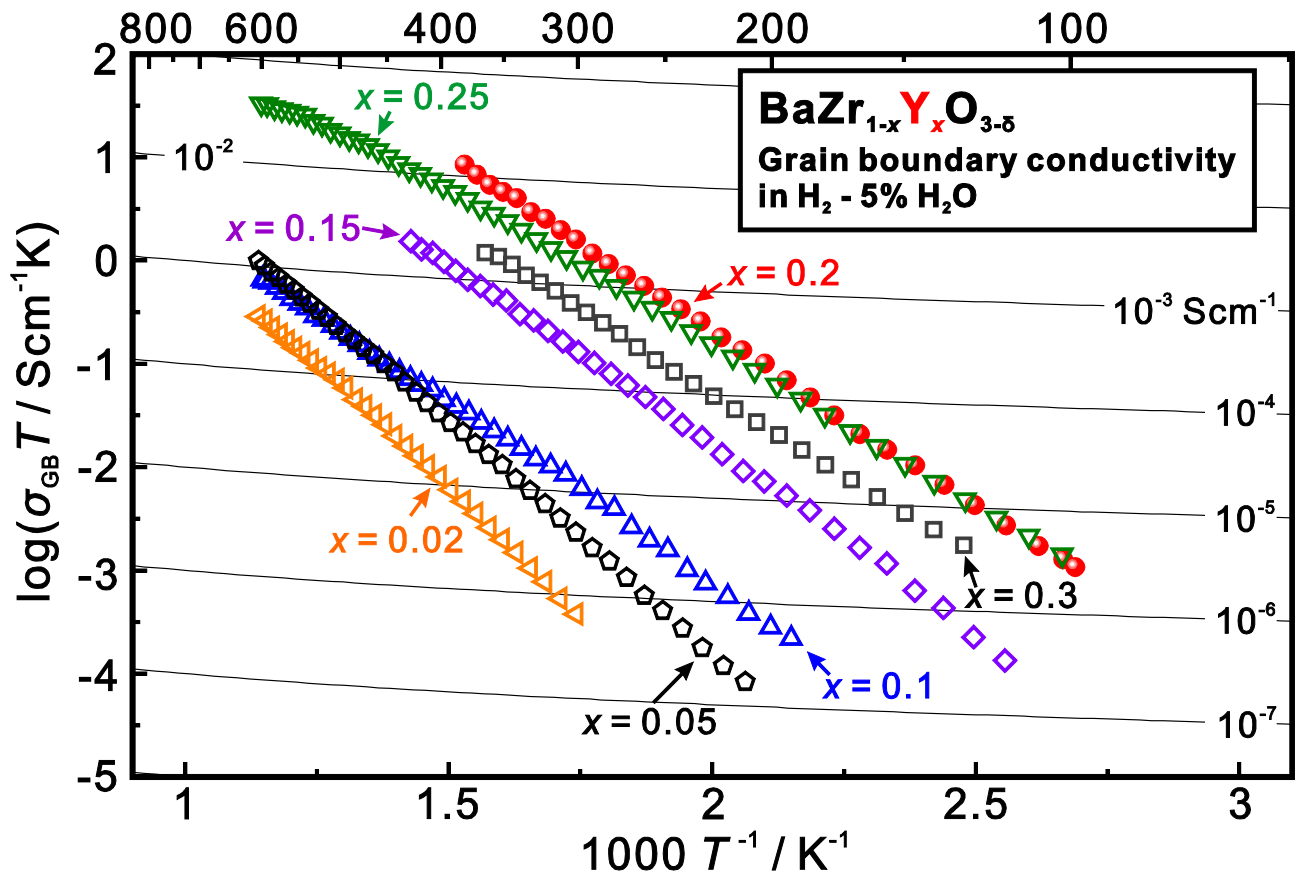
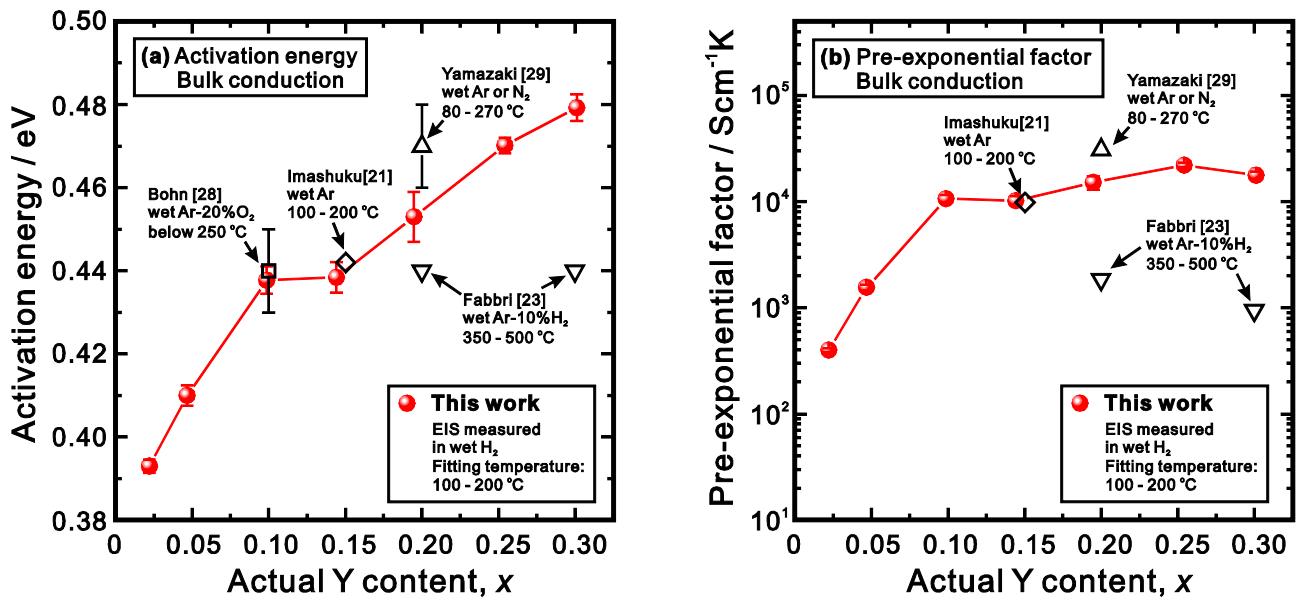**Fig. 9** Arrhenius plots of grain boundary conductivities of $BaZr_{1-x}Y_xO_{3-\delta}$ (x = 0.02, 0.05, 0.1, 0.15, 0.2, 0.25 and 0.3) in wet H_2 atmosphere with the water vapor pressure of 0.05 atm. All the samples were finally heat-treated at 1600 °C in O_2 for 24 h for sintering.
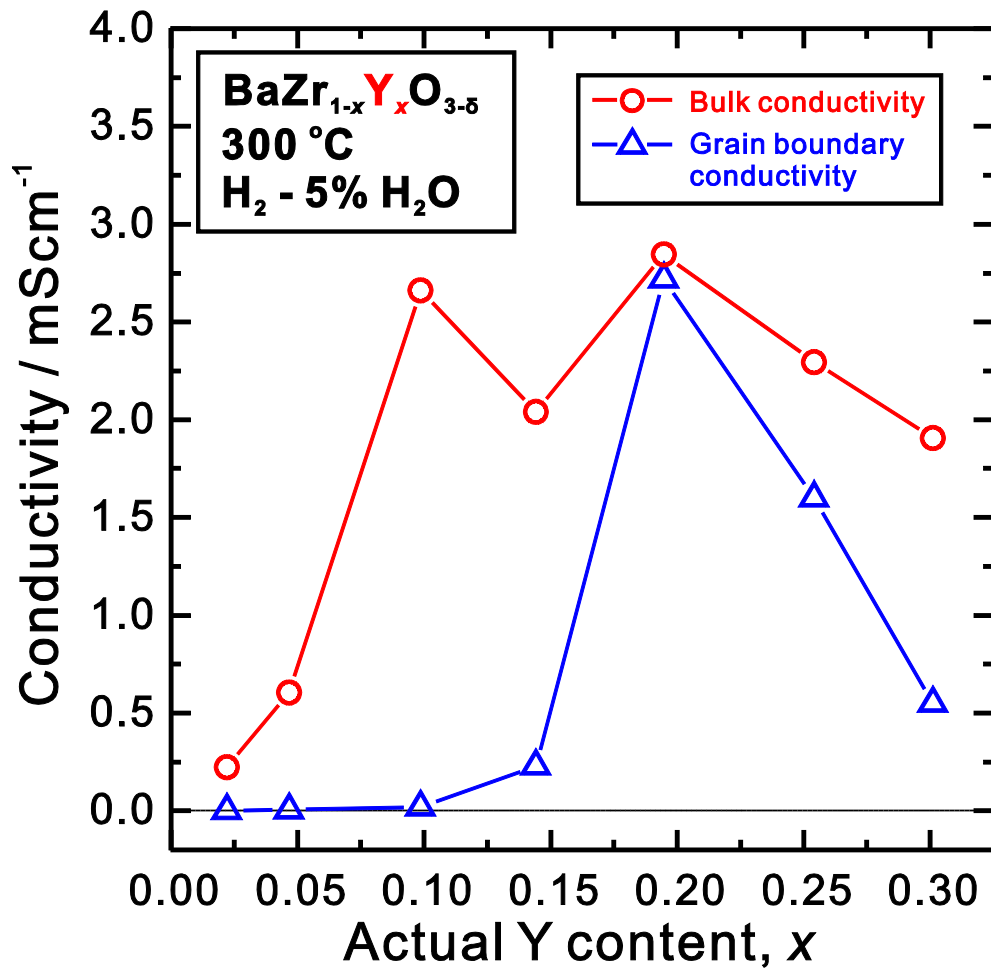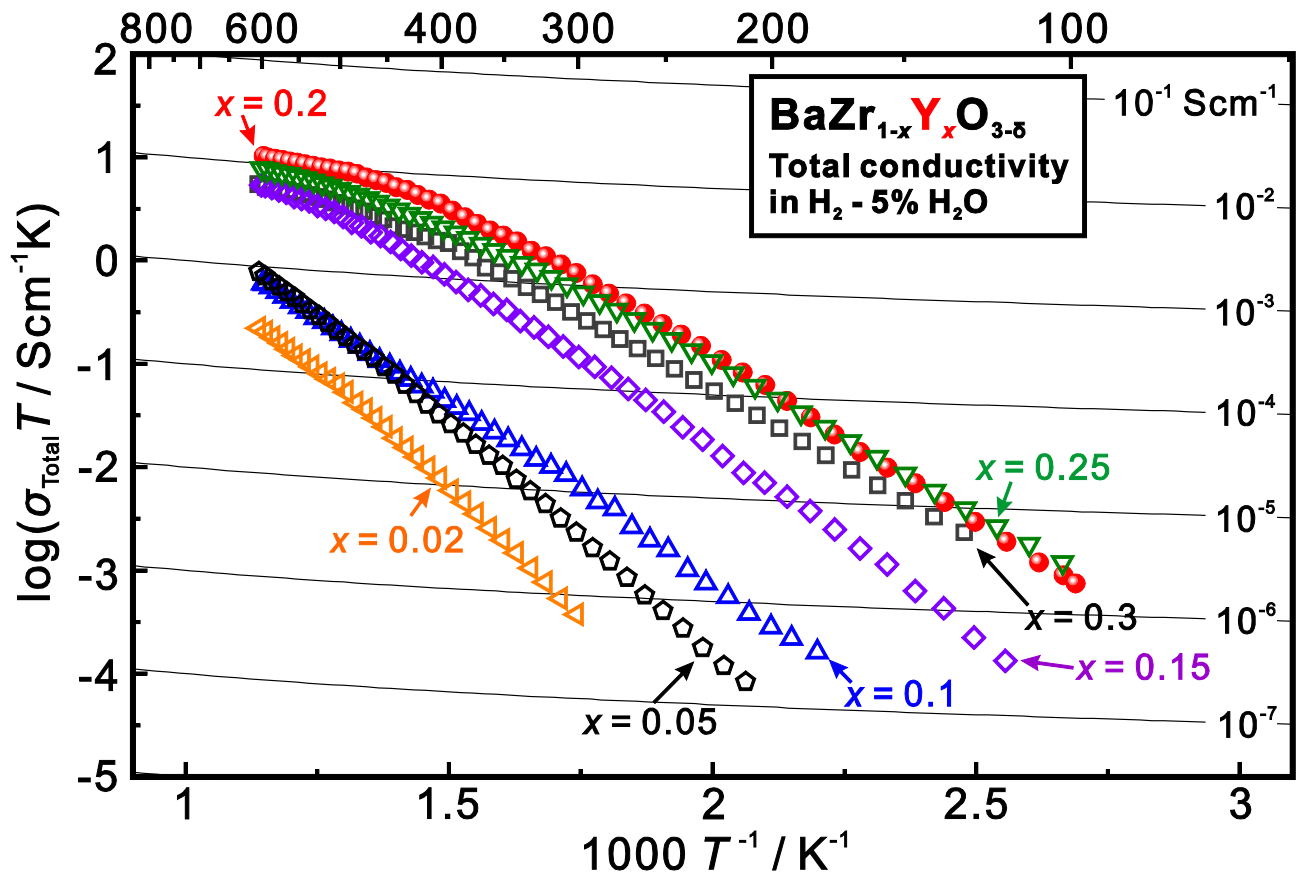
Fig. 10   Bulk conductivity and effective grain boundary conductivity of $BaZrO_3$ doped with various

Y content at 300 ºC in wet H_2 (p_{H_2O} = 0.05 atm) plotted against the actual Y content determined by

ICP-AES H_2 – 5% H_2O atmosphere.

Fig. 11 (a) Activation energy and (b) pre-exponential factor of bulk conduction of BaZrO₃ doped with various amount of Y plotted against the actual Y content determined by ICP-AES. The activation energy and pre-exponential factor were obtained by fitting the bulk conductivity measured in the temperature range around 100 – 200 °C in H_2 – 5% H_2O atmosphere. Literature data [21, 23, 28, 29] were also plotted for comparison.

Fig. 12 Arrhenius plots of total conductivities of $BaZr_{1-x}Y_xO_{3-\delta}$ (x = 0.02, 0.05, 0.1, 0.15, 0.2, 0.25 and 0.3) in wet H_2 atmosphere with the water vapor pressure of 0.05 atm. All the samples were finally heat-treated at 1600 $^\circ$C in O_2 for 24 h for sintering.
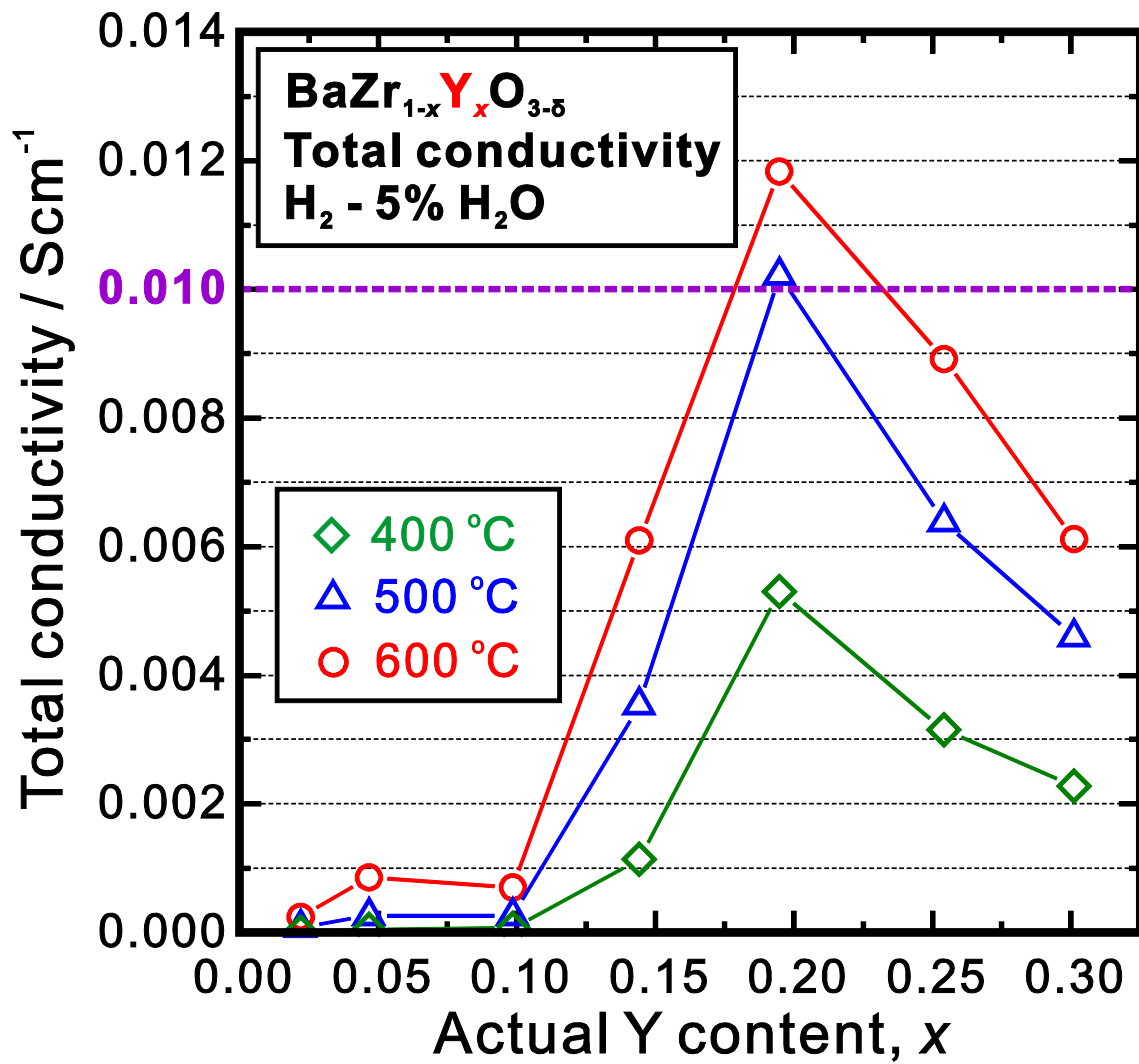
Fig. 13 Total conductivity of BaZrO$_3$ doped with various Y content at 400, 500 and 600 $^\circ$C in wet

H$_2$ (p_{H_2O} = 0.05 atm) plotted against the actual Y content determined by ICP-AES. Violet dash

line indicates the ionic conductivity of 0.01 Scm^{-1} necessary for an applicable electrolyte in fuel cells.

[30]
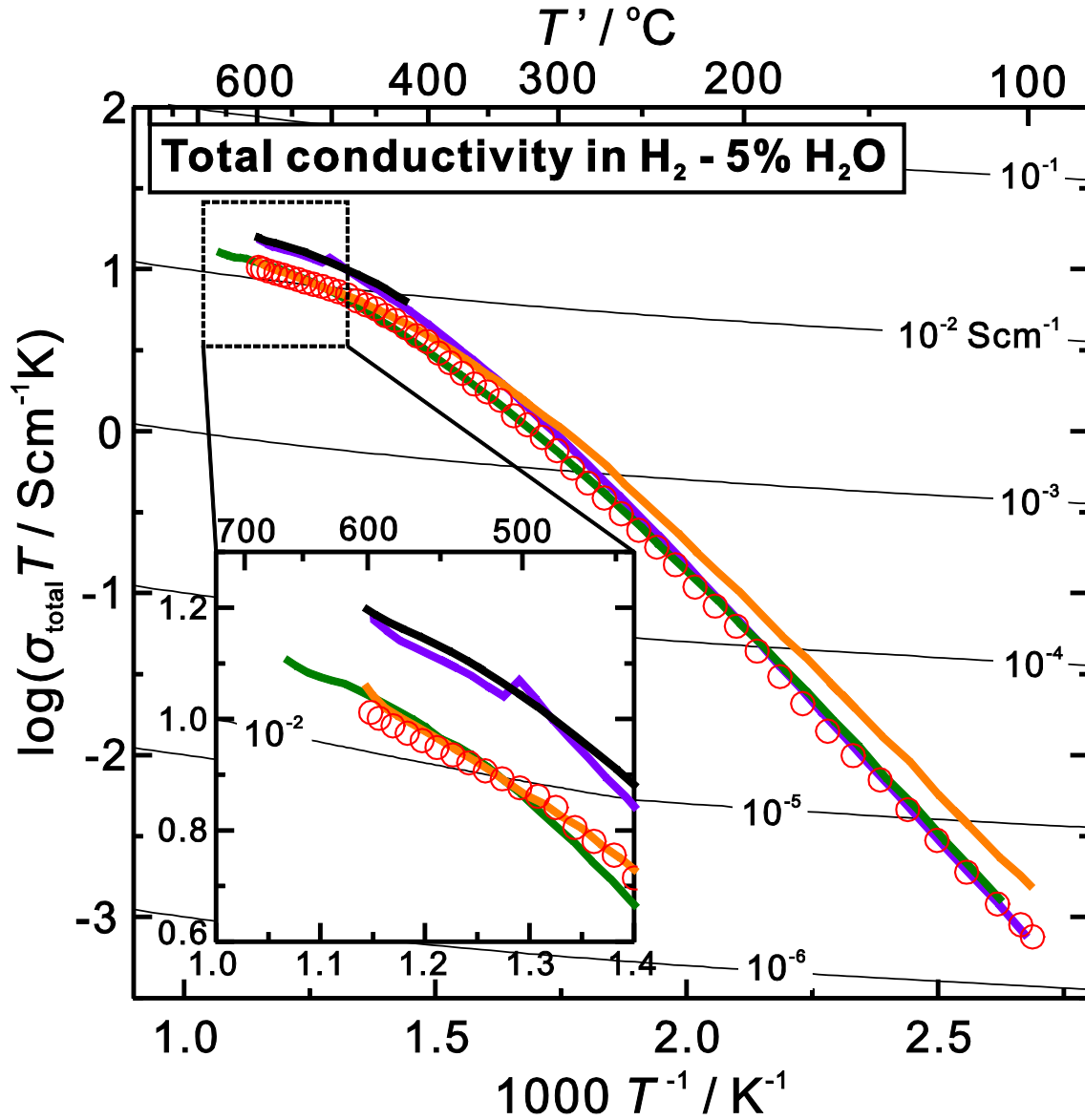
Fig. 14 Total conductivity in H_2 – 5% H_2O of $BaZr_{0.8}Y_{0.2}O_{3-\delta}$ sintered at five different batches.

The data marked with circle symbols are those plotted in **Fig. 12**.